Journal of Power Sources 250 (2014) 21–29

Contents lists available at ScienceDirect

Journal of Power Sources

journal homepage: www.elsevier.com/locate/jpowsour

An experimental investigation of pressurized planar solid oxide fuel cells using two different flow distributors

H.W. Chang, C.M. Huang, S.S. Shy*

Department of Mechanical Engineering, Center for Energy Research, College of Engineering, National Central University, Jhong-li 32001, Taiwan

HIGHLIGHTS

- A high-pressure dual-chamber facility is established for pressurized SOFC studies.
- Electrochemical impedance spectra of PSOFC using single-cell stacks are measured.
- These EIS data explain why and how the cell performance is increased with pressure.
- This study is useful to the development of PSOFC integrating with micro gas turbines.

ARTICLE INFO

Article history:
Received 21 June 2013
Received in revised form
13 October 2013
Accepted 17 October 2013
Available online 7 November 2013

Keywords:
Pressurized solid oxide fuel cell
Flow distributors
Flow uniformity
Cell performance
Electrochemical impedance spectra
Ohmic and polarization resistances

ABSTRACT

A high-pressure high-temperature dual-chamber facility is established for electrochemical impedance measurements of pressurized solid oxide fuel cells (PSOFC) to explain why and how the cell performance is increased with increasing pressure (p). By comparing two sets of nearly identical single-cell stacks except using different flow distributors with different degrees of flow uniformity at 850 °C over a range of p varying from 0.1 MPa to 0.5 MPa, we found that the better flow uniformity in flow distributors is, the better the cell performance is, and such performance enhancement is increased with increasing p. This finding is explained by impedance spectra and their associated equivalent circuit models, showing the coupling impact of flow uniformity and pressure elevation to the decrease of ohmic and polarization resistances. These results should be useful to the development of PSOFC integrating with micro gas turbines for future stationary power generation.

1. Introduction

Keeping pace with a rapid increase in population, prosperity, and the desire for improving the quality of life, the demand for electricity as the major form of applicable energy in our modern society has been drastically increased over the past. In the beginning of twenty century, only 1% of all fossil primary energy was converted to electricity, but in recent years this has been increased worldwide to about 40% [1,2]. Further, such increasing trend is expected to rise in relation to the advances of the gross national product in the future. The excessive consumption of energy and natural resources, deforestation, land use and land cover changes, and air, land and water pollution caused by human activities had unfortunately already put tremendous impact on the Earth. Nowadays, we are facing many serious environmental and energy shortage problems. Delay of action will jeopardize the ability of future generations to meet their needs. Hence, highly efficient power generation systems with very low emissions are urgently needed in our modern society. Among a few potential candidates, the hybrid system including a pressurized solid oxide fuel cell (PSOFC) integrating with a gas turbine or micro gas turbine (MGT) has the highest efficiency [3–12]. This motivates the present study to measure the detail electrochemical characteristics of PSOFC which is the essential component of the hybrid system.

The hybrid PSOFC–MGT power system may be expected to reach efficiencies approaching up to 70% [3]. Such a highly efficient synergetic technology not only has great potential for reducing the fuel consumption and the capital cost per unit power output [3–11], but also it has a very wide range of applications from some 10 kW to multi MW [12]. Thus, the PSOFC–MGT system is important to the advance of the fuel cell technology as well as for the expansion of the gas turbine industry. There are a few demo

* Corresponding author. Fax: +886 3 427 6157.
E-mail address: sshy@ncu.edu.tw (S.S. Shy).

0378-7753/$ – see front matter © 2013 Elsevier B.V. All rights reserved.
http://dx.doi.org/10.1016/j.jpowsour.2013.10.127

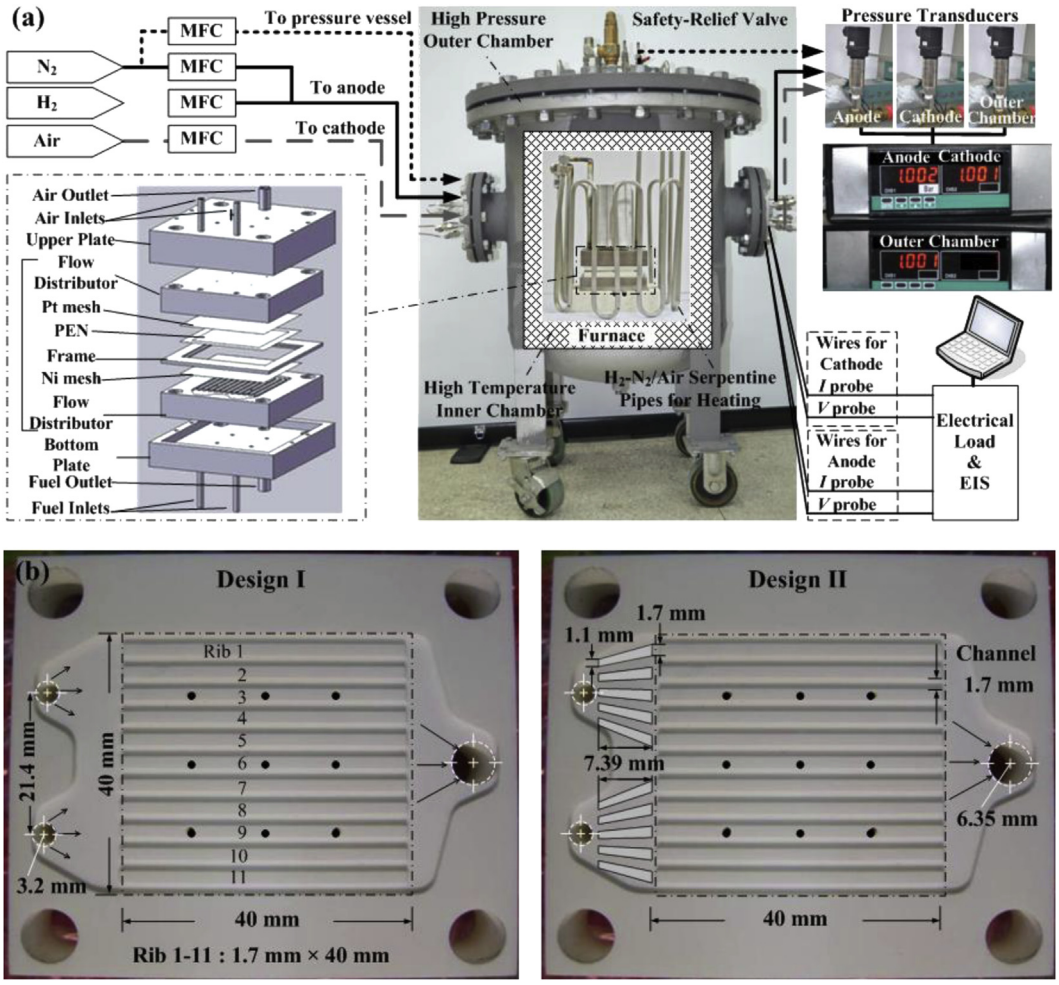

Fig. 1. (a) A high-pressure double-chamber planar solid oxide fuel cell testing platform. (b) Two flow distributors, designs I and II.

examples available for the hybrid PSOFC–MGT power system deserving to mention. For instances, Siemens had showed the feasibility with its 220 kW PSOFC–MGT hybrid system (PH220) [6], the Korea Institute of Energy Research tested a 30 kW (5 kW PSOFC integrated with 25 kW MGT) hybrid system [7], Mitsubishi Heavy Industries manufactured a 200-kW class hybrid PSOFC–MGT combined-cycle power plant and conducted a performance test in 2007 [8], and the German Aerospace Center (DLR) has started a project aiming to demonstrate a 50 kW hybrid PSOFC–MGT power system [12]. Though these demo examples are successful in some measure, many technical challenges in designing the hybrid power system and its control still remain to be solved before the safe and stable operation of PSOFC–MGT power generation system among different components can be assured to make the industrial application feasible. One of the most important technical challenges is the knowledge of the electrochemical characteristics of PSOFC. So far in the available literature, there are very few experimental data of electrochemical impedance spectra (EIS) for the PSOFC stack [12]. Hence, the objective of this study is to establish a high-pressure double-chamber testing platform for measurements of the PSOFC using a single-cell stack setup (a full cell with interconnectors) at elevated pressure (p) up to 0.6 MPa and thus the wanted EIS data can be measured for the first time.

The "single-cell stack" term has already been used by several research groups [e.g., [13–17]], which not only includes a "single cell" consisting of a positive electrode-electrolyte-negative electrode (PEN) and current collectors but also has flow distributors (interconnectors) in both anode and cathode. Previous studies under atmospheric pressure condition [15,16] applied various designs of commonly-used rib-channel flow distributors having different degrees of flow uniformity to measure the impact of flow uniformity in interconnectors on power generating characteristics of single-cell stacks. It was found that by improving flow uniformity in interconnectors can result in more than 10% increase of the cell power density without pressurization [15,16]. Such finding was further explained by the corresponding EIS measurements [17], in which the EIS data clearly showed that both ohmic and polarization resistances are smaller for the case of better flow uniformity in interconnectors. In the present study, we apply the same single-cell stacks as that previously used in Refs. [15–17] but with new modifications for conducting high-pressure SOFC experiments as to be discussed in detail. In short, we aim to measure the impact of flow uniformity in interconnectors on the cell performance and electrochemical characteristics of single-cell stacks under elevated pressure conditions, so that the following questions may be addressed. How exactly would the power generating characteristics of anode-supported single-cell stacks vary with a change of pressurization? What is the effect of flow uniformity in interconnectors on the cell performance and electrochemical impedance spectra of single-cell stacks at elevated pressures? Can the measured EIS data of single-cell stacks under both unloaded and loaded conditions over a range of pressure be used to explain quantitatively the coupling influence of pressurization and flow uniformity in interconnectors on the cell performance of PSOFC? It should be noted

again that so far little EIS information is available for PSFOC under loaded conditions.

The organization of the paper is as follows. The next section presents a high-pressure double-chamber test rig for the study of PSOFC. In it two sets of nearly identical single-cell stacks except using different flow distributors with different degrees of flow uniformity are tested. Furthermore, the arrangements of power and EIS measurements used in the present high-pressure study are described. Section 3 presents the aforesaid two complete data sets of power-generating characteristics of high-pressure single-cell stacks using different flow distributors, showing the effects of pressurization and flow uniformity in interconnectors on the cell performance of PSOFC. Following that results of high-pressure EIS data obtained under both unloaded and loaded conditions using two different flow distributors are presented in Section 3.2, such that a better understanding of the knowledge of the electrochemical characteristics of PSOFC can be obtained. Finally, the conclusions of the present PSOFC study are summarized in Section 4.

2. Experimental arrangement and measurement

Fig. 1a presents a high-pressure double-chamber testing platform for cell performance and electrochemical impedance spectra measurements of single-cell stacks using two different flow distributors for the PSOFC study. Note that the two rib-channel flow distributors, as shown in Fig. 1b as indicated by designs I and II, are exactly the same except that the design II applies 10 small guide vanes equally positioned around the double-inlet feed header. Hence, the dimensions of widths and lengths as indicated in Fig. 1b at different locations are applicable for both designs. As seen from the central part of Fig. 1a, a program-controlled tubular furnace (the inner chamber) is resided in a relatively large pressurized chamber (the outer chamber). Inside the inner furnace, there is a testing single-cell stack. For clarity, an exploding sketch of the single-cell stack is depicted on the left bottom part of Fig. 1a. The assembly of the single-cell stack is essentially the same as our previous SOFC studies under normal pressure condition [15–17]. In it an anode-supported PEN purchased from H.C. Starck (ASC 3) having an effective reactive area of 40 × 40 mm^2 that is 16 times larger than that of commonly-used button cells, a supporting metallic frame made of crofer 22-APU, and the current collectors are sandwiched by a pair of rib-channel flow distributors (interconnectors) in both anode and cathode to form a single-cell stack (please see the exploding sketch in Fig. 1a). The usage of the metallic frame is to provide the mechanical support to the PEN and to further prevent

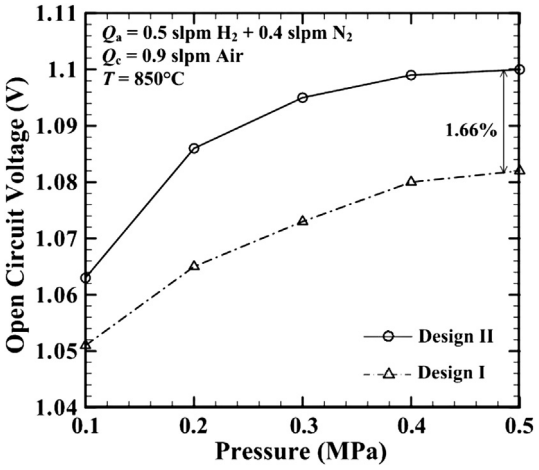

Fig. 2. Measured values of OCV plotted against pressure for these two nearly-identical single-cell stacks except using different flow distributors (designs I and II).

the possible cross-leakages between fuel and oxidant from both feed and exhaust headers of flow distributors. The new modifications are the arrangement of the serpentine pipes in the inner furnace (see the central inset picture of Fig. 1a) and its associated flow controllers and valves in order to achieve uniform temperature distributions in both anode and cathode. This arrangement is essential for a successful PSOFC operation, because if the gas supply lines in the inner furnace are too short in lengths, the supplied gases cannot be sufficiently heated before they enter the anode and the cathode. Consequently, the cooler gases can produce non-uniform temperature distributions in the anode and the cathode resulting in a failure of PSOFC. In addition, the upper and lower flow distributors (Fig. 1b) are fabricated by aluminum oxide materials to keep away from the poisoning problem of the electrodes due to the chromium volatilization from the metallic flow distributors. On the left top part of Fig. 1a, three supply gas lines together with their corresponding mass flow controllers are indicated, where N_2 gas is used to pressurize the outer pressure vessel, air is used in the cathode, and H_2 and N_2 gases with various mixture fractions are used in the anode. On the right top part of Fig. 1a, there are three pressure transducers which are used to monitor and control pressure inside the anode, the cathode, and the outer chamber. For simplicity, we only schematically show the current and voltage wires of both anode and cathode connecting to a Prodigit 3310D electronic load controlled by a data acquisition computer for measurements of power generating characteristics (see the right bottom part of Fig. 1a). As to the electrochemical impedance spectra measurements, the reader is directed to Ref. [17] for a detail treatment on the connecting wires of both anode and cathode to the EIS measuring device. All data, such as temperatures, voltages, pressures, and mass flow rates, are continuously monitored and analyzed by the computer using LabView software.

Two flow distributors (designs I and II) are applied as shown in Fig. 1b, of which both designs have the same double-inlet/single-outlet rib-channels including 11 ribs and 12 flow channels with exactly the same dimensions. But only the design II applies 10 small guide vanes equally positioned around the double-inlet feed header. All relevant dimensions of the two flow distributors are also indicated on Fig. 1b; however, for detail treatment, the reader is directed to Ref. [15,16]. Note that the design I has a poor flow uniformity in interconnectors, while the design II has an excellent flow uniformity in interconnectors because of using guide vanes around the feed header (Fig. 1b), as already validated by experimental measurements and numerical simulations [15–17]. To test how the impact of flow uniformity in interconnectors on the cell performance of single-cell stacks would vary with an increase of pressure, the same testing procedures as that used previously at 0.1 MPa [17,18] are applied except that experiments are conducted in the double-chamber facility with serpentine heating pipes under elevated pressure conditions. The test procedures include a 24-h anode reduction, the start-up procedure, and the data taking process while keeping the same flow rates in both anode and cathode for unloaded and loaded conditions, as can be found in Refs. [16,17]. In this paper, we will report two complete data sets of power densities and impedance spectra of single-cell stacks using different flow distributors (design I and II; Fig. 1b) over a range of p varying from 0.1 MPa to 0.5 MPa, where the experimental conditions are kept the same. In other words, the same flow rates are applied (Q_{anode} = 0.5 slpm H_2 + 0.4 slpm N_2 and $Q_{cathode}$ = 0.9 slpm air) and the same operating temperature is also used (T = 850 °C). Hence, by directly comparing these two data sets of experiments with different degrees of flow uniformity in interconnectors under elevated pressure conditions, the coupling influence between pressurization and flow uniformity on the performance of PSOFC may be scrutinized.

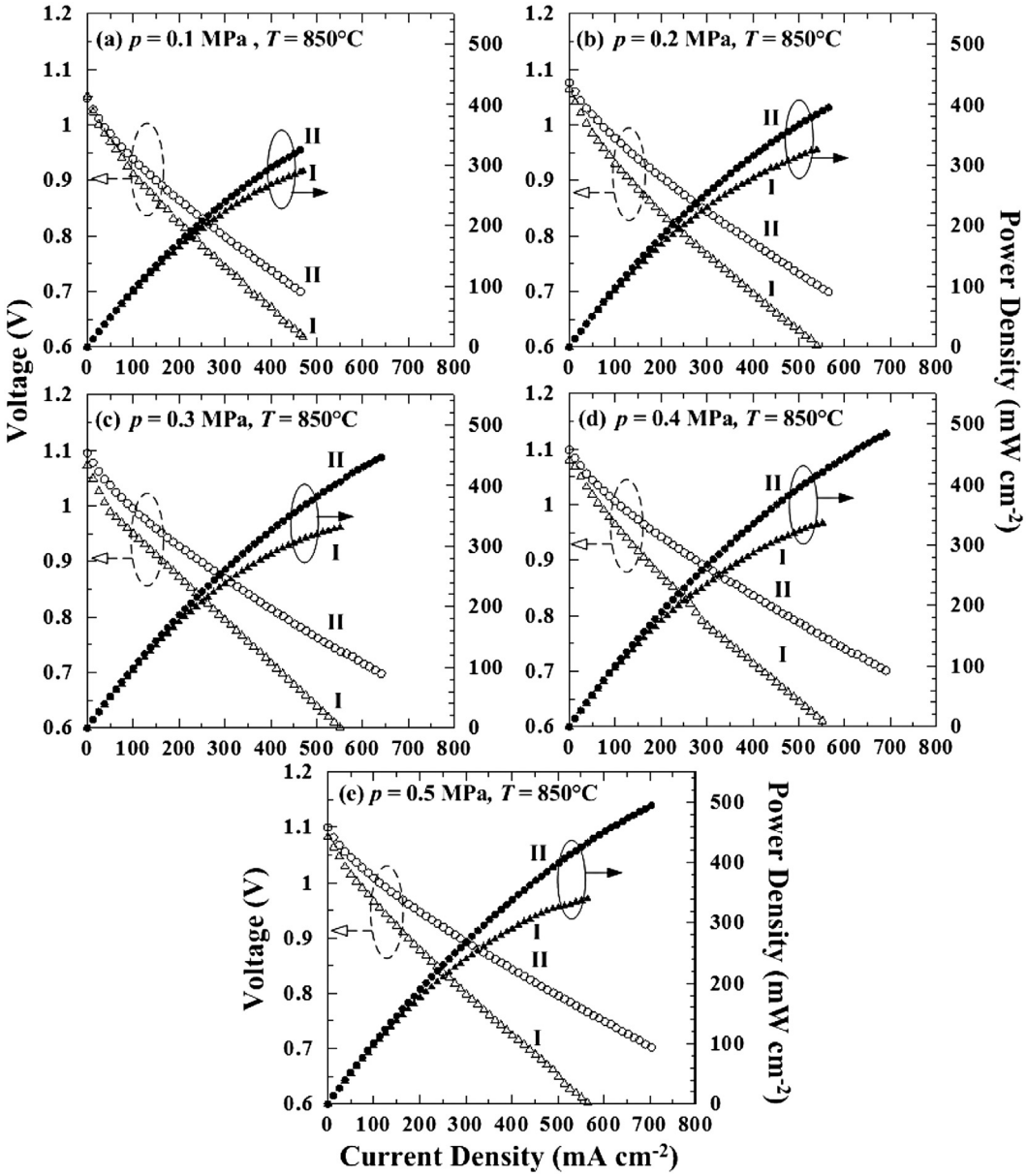

Fig. 3. Comparisons of measured power-generating characteristics between the two nearly-identical single-cell stacks except using different designs of flow distributors (designs I and II) under different operating pressures varying from 0.1 MPa to 0.5 MPa.

As to the electrochemical impedance spectra measurements, the present study applies an AC impedance analyzer (Bio-Logic, model SP-150) together with a current amplifier (Biologic, VMP3) to measure the impedance spectra of the aforementioned two single-cell stacks using different interconnectors with different degrees of flow uniformity under elevated pressure conditions (p = 0.1–0.5 MPa). The current amplifier is used to enlarge the measuring range of the operating current from ±800 mA to ±20 A. Because the PEN of the present single-cell stack has a square shape (not a circular shape for the small button cell), it is rather difficult to employ a reference electrode on its perimeter. Therefore, we apply a two-electrode arrangement for EIS measurements that is the same as that used in Ref. [17], of which both the counter electrode and the reference electrode from the current amplifier and the EIS device are connected with the current collector in the cathode side of the single-cell stack. For detail treatment on the AC impedance measurements, especially on how to connect the positive electrode (cathode) and the negative electrode (anode) of the single-cell stack, the reader is directed to Ref. [17]. On both anode and cathode surfaces, eight platinum wires equally spaced on these surfaces are used to collect uniformly the impedance data from the anode-supported single-cell. We apply an AC sinusoidal-wave potential perturbation with a signal amplitude of 20 mV to measure the corresponding current response of the single-cell stacks under elevated pressure conditions. In the present PSOFC study, the impedance spectra are measured at two different DC conditions, at open circuit voltage (OCV) and at 0.7 V, each covering a range of frequency from 50 mHz to 3 kHz.

3. Results and discussion

3.1. Power generating characteristics of PSOFC using different flow distributors

Fig. 2 shows variations of measured OCV with increasing pressure for the aforementioned two sets of nearly identical single-cell

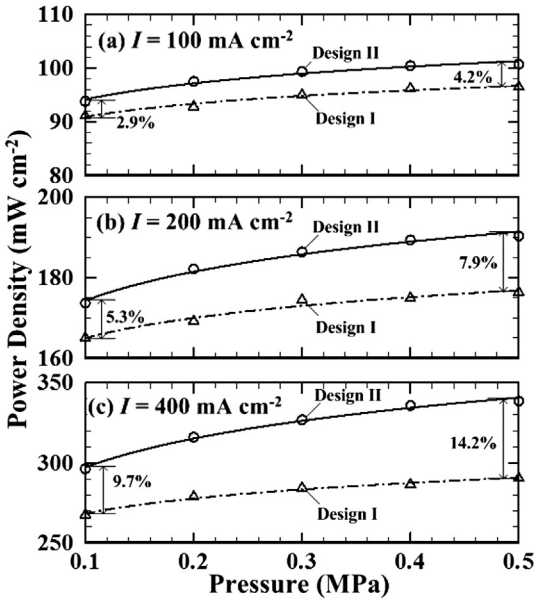

Fig. 4. Same power density data taking from Fig. 3 at three fixed current densities: (a) 100 mA cm^{-2}, (b) 200 mA cm^{-2} and (c) 400 mA cm^{-2}, plotted against pressure, showing the impact of flow uniformity in interconnectors under various elevated pressure conditions.

stacks except that only the design II case applies ten small guide vanes in the feed header of flow distributors having a much better flow uniformity than the design I case (please see Fig. 1b), where the experimental conditions for both designs I and II cases are kept the same. There are three points in Fig. 2 deserving comments. First, the values of OCV for both designs are found to be increased with increasing pressure. Specifically, when p increases from 0.1 MPa to 0.5 MPa at $T = 850$ °C, an OCV increase of about 31 mV for the design I case and/or 37 mV for the design II case is measured. It is reasonable to suggest that the increase of OCV is due to the decrease of both activation and concentration overpotentials in the anode as p is increased. Secondly, the increasing trend of values of OCV is found to be more significant from 0.1 MPa to 0.3 MPa as compared to those values at higher p (0.4 and 0.5 MPa), where a more modest increment is measured, suggesting a bending effect of the OCV curve at higher values of p. Thirdly, it is found that at any pressures studied, measured values of OCV for the design II using guide vanes are higher than that of the design I without using guide vanes, having an increment of 1.66% at $p = 0.5$ MPa as indicated on Fig. 2. This is attributed to the better flow uniformity in interconnectors for the design II case.

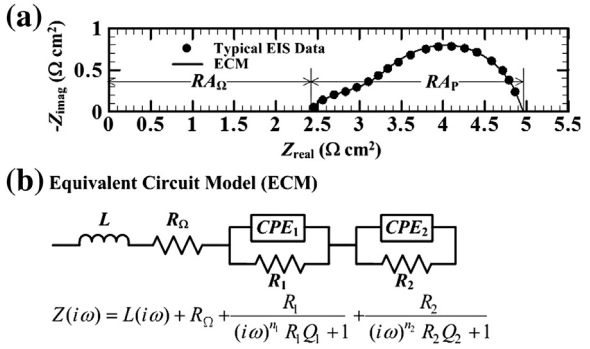

Fig. 5. (a) A typical impedance spectrum data points obtained at OCV using the design II interconnector together with the associated equivalence circuit model (ECM) curve line, showing the determination of ohmic and polarization resistances (RA_Ω and RA_P) along the real axis (Z_{real}). (b) The equivalent circuit model to fit the present experimental data.

In order to show the power-generating characteristics under loaded and pressurized conditions as well as the comparison between designs I and II, the measured I–V curves and their corresponding power densities for both cases are presented in Fig. 3 together using the same scales in both x and y axes, each case including five different pressures varying from 0.1 MPa to 0.5 MPa. Note that the measurements start from the zero current for the OCV and then increase the current density load incrementally (each increment of 12.5 mA) until that the operating voltages reach at 0.7 V for the design II and/or at 0.6 V for the design I due to the poorer performance in the latter case. By comparing these two data sets (designs I and II), it can be seen that the design II having a better flow uniformity in flow distributors has a better cell performance than that of the design I for all five different pressures studied. More importantly, such cell performance enhancement, a result of improving flow uniformity in interconnectors, is found to be even more profound at higher p, as can be seen by comparing these five data sets at different p in Fig. 3. To further evaluate quantitatively the aforesaid cell performance enhancement owing to the influence of flow uniformity, Fig. 4 plots the same power density data taken from Fig. 3 at three fixed current densities (100, 200 and 400 mA cm^{-2}) against pressure. At $I = 100$ mA cm^{-2}, the power densities of the design II case are larger than that of the design I case with an increment percentage of 2.9% at $p = 0.1$ MPa and 4.2% at $p = 0.5$ MPa, showing the impact of flow uniformity and the effect of pressurization as indicated in Fig. 4a. Note that such increment percentages between designs II and I increase with increasing values of I, for instances from 5.3% at $p = 0.1$ MPa to 7.9% at $p = 0.5$ MPa when $I = 200$ mA cm^{-2} (Fig. 4b) and from 9.7% at $p = 0.1$ MPa to 14.2% at $p = 0.5$ MPa when $I = 400$ mA cm^{-2} (Fig. 4c). These results not only show how exactly the single-cell stacks' power densities vary with increasing pressure (Fig. 3), but also provide the increasing percentages of power densities due to the impact of flow uniformity in interconnectors between designs II and I (Fig. 4).

Pressurization of SOFC is beneficial, because the power densities can be increased, as shown in Figs. 3 and 4. This can be understood from the effect of pressurization on anodic activation and concentration overpotentials. As p increases, the anodic fuel gas density increases, both molar concentration and diffusion rate increase, and thus the porous electrode becomes more reactive, leading to lower activation and concentration overpotentials. Furthermore, to the cathode side, the partial pressure of oxygen (p_{O2}) is directly proportional to the net pressure of air, so that the higher p_{O2} is, the higher the cell performance is. However, p_{O2} is independent of the net pressure of the anodic gases, because p_{O2} depends on the ratio of p_{H2O}/p_{H2} (or p_{CO2}/p_{CO}) which is independent of the net pressure.

3.2. Impedance spectra of PSOFC using different flow distributors

Before we discuss measured impedance spectra data for the single-cell stacks using two different flow distributors under elevated pressure condition, a typical measured impedance spectrum together with an equivalent circuit model (ECM) for best fitting the measured impedance data are first described in Fig. 5 in order to demonstrate the determination of ohmic and polarization resistances which are to be used to explain why and how the cell performance of PSOFC increases with increasing pressure.

Fig. 5a is the well-know Nyquist plot, in which the wanted information of the general ohmic and polarization resistances (RA_Ω and RA_P) can be extracted. For clarity, this is indicated by the intersecting points of the impedance arcs on the real axis of Fig. 5a.

Table 1
Various key elements used in the proposed equivalent circuit model for designs I and II at (a) OCV (Fig. 6) and (b) 0.7 V (Fig. 7).

ECM elements	p = 0.1 MPa		p = 0.2 MPa		p = 0.3 MPa		p = 0.4 MPa		p = 0.5 MPa	
	I	II	I	II	I	II	I	II	I	II
(a) OCV										
L (μH)	0.7996	0.7046	0.8272	0.7057	0.7600	0.7347	0.7600	0.6578	0.7778	0.7346
R_Ω (Ω)	0.2934	0.2105	0.2736	0.2105	0.2725	0.2096	0.2705	0.2155	0.2776	0.2197
Q_1 (Fs^{n1-1})	0.1184	0.5831	0.2759	0.6679	0.3027	0.8791	0.4040	1.7600	0.1790	1.7740
n_1	0.6030	0.4824	0.4992	0.4724	0.5038	0.4323	0.4699	0.4326	0.5308	0.4547
R_1 (Ω)	0.0541	0.0406	0.0484	0.0302	0.0431	0.0266	0.0410	0.0221	0.0399	0.0206
Q_2 (Fs^{n2-1})	1.5740	3.0400	2.1660	3.8100	2.1620	5.2310	2.8170	6.2410	1.9350	6.7360
n_2	0.8726	0.9665	0.8454	0.8958	0.8697	0.8396	0.8268	0.8302	0.8288	0.8135
R_2 (Ω)	0.0259	0.0200	0.0215	0.0189	0.0200	0.0180	0.0188	0.0176	0.0180	0.0174
(b) 0.7 V										
L (μH)	0.8254	0.8211	1.1560	0.8439	1.0540	0.8100	0.8798	0.7671	1.0890	0.7227
R_Ω (Ω)	0.2926	0.2059	0.2739	0.2063	0.2745	0.2083	0.2715	0.2126	0.2812	0.2178
Q_1 (Fs^{n1-1})	1.9440	0.3995	2.8460	0.5275	3.5780	1.1940	4.2960	2.8580	4.5400	3.1090
n_1	0.5414	0.4439	0.4558	0.4126	0.4350	0.3472	0.4199	0.3012	0.4397	0.3134
R_1 (Ω)	0.0476	0.0379	0.0432	0.0331	0.0418	0.0305	0.0404	0.0288	0.0396	0.0270
Q_2 (Fs^{n2-1})	0.0387	4.3220	0.0043	6.0120	0.0077	9.2520	0.0344	13.9700	0.0035	21.0500
n_2	0.6902	0.7542	0.9125	0.7712	0.8793	0.7823	0.7203	0.7773	1.0000	0.0208
R_2 (Ω)	0.0343	0.0188	0.0272	0.0158	0.0223	0.0129	0.0216	0.0109	0.0109	0.0100

Note that values of RA_Ω and RA_P are multiplied by the effective anodic reactive surface area A_{eff} (=16 cm^2) having a unit of Ω cm^2. Further, the total impedance, $RA_{tot} = RA_\Omega + RA_P$, is usually composed of a number of basic lumped elements, including such as the inductors (L), the capacitors (Q), and the resistors (R) in series or in parallel and/or in a combination of both. Therefore, RA_{tot} can be mathematically represented by $Z(i\omega) = Z_L + Z_R + Z_{RQ1} + Z_{RQ2}$ (see Fig. 5b) for the present single-cell stacks under elevated pressure condition. The first term $Z_L = L(i\omega)$ is the induction impedance that is contributed from the device's electromagnetic induction. Then the ohmic impedance $Z_R = R_\Omega$, the second term, is contributed by ions and/or electrons transferring in the electrolyte and/or conductor, which is independent of frequency and can be directly determined from the first intersecting point of the impedance arcs along the real axis of the Nyquist plot. The last two terms are $Z_{RQj} = R_j/[(i\omega)^{nj}R_jQ_j + 1]$ where the subscript j = 1, 2, indicating various contributions from the non-uniform distribution of reaction rates, the electrodes' porosity and/or the surface roughness and compositions [19], which are frequency-dependent elements having only the imaginary contribution. Moreover, the present single-cell stacks apply two constant-phase elements (CPEs), as indicated by CPE_1 and CPE_2 in Fig. 5b, to model the measured EIS data consisting of two overlapping arcs or semicircles with their centers positioned at the real axis (see Fig. 5a). Such an ECM (Fig. 5b) is used to best fit the present measured impedance spectra for these two sets single-cell stacks using different flow distributors over a range of pressure varying from 0.1 MPa to 0.5 MPa. For clarity, all values of key parameters and elements in the ECM are listed in Table 1 for both unloaded and loaded conditions. Hence, the extracted information of ohmic and polarization resistances from the measured EIS data can be used to explain the effect of pressurization and the impact of flow uniformity in interconnectors on the performance of PSOFC, as discussed below.

Figs. 6 and 7 present the EIS data respectively at unloaded (OCV) and loaded (0.7 V) conditions. Each of two figures includes five Nyquist plots at five different pressures varying from 0.1 MPa to 0.5 MPa, where the data of both designs I and II are plotted together using the same scales for comparison. There are two key points. First, all measured impedance data, as represented by the triangle (design I) and circle (design II) symbols scanning from ~0 Hz on the right end to the highest frequency (~3Kz) on the left end in Figs. 6 and 7 under unloaded and loaded conditions, appear to have a similar shape consisting of two overlapping semicircles. Thus, these measured impedance data can be well fitted by the proposed ECM (see also Fig. 5b and Table 1) that is represented by the solid lines in the Nyquist plots of Figs. 6 and 7. Secondly, the impedance arcs of the design II are found to be smaller than that of the design I at any fixed p ranging from 0.1 MPa to 0.5 MPa under both unloaded and loaded conditions. In other words, at both OCV (Fig. 6) and 0.7 V (Fig. 7) conditions, the cases using the design II with higher flow uniformity in interconnectors have lower values of RA_Ω and RA_{tot} than that of the cases using the design I at any given pressures. A question may be raised. Why do values RA_Ω in the case of design I be larger than that in the case of design II? We anticipate that the reason is due to the occurrence of the anodic re-oxidation in the case of design I. This is because the case of design I has non-uniform flow distributions in interconnectors that may lead to non-uniform fuel utilization rates in the surface of the anode. At some points or areas in the anode having a high fuel utilization rate, the local fuel starvation may be occurred that can lead to the anodic re-oxidation. When the anodic re-oxidation occurs, it can change the local anodic microstructures (Ni becomes NiO) during the operation of PSOFC, block the mass diffusion pathway of supplied fuel gases under either normal or elevated pressure conditions, and thus increase values of RA_Ω. Such an anodic re-oxidation does not occur in the case of design II because flow distributions in interconnectors are uniform. This may explain why values of RA_Ω in the case of design II are smaller than that on the case of design I.

To clearly show the quantitative variations on the ohmic and polarization resistances at five different pressures under both OCV and 0.7 V conditions, Figs. 8 and 9 present the corresponding values of RA_Ω and RA_P extracted from Figs. 6 and 7 as a function of p for both designs I and II. At the OCV condition, values of RA_Ω remain a constant of 2.55 Ω cm^2 for the design II and/or 3.13 Ω cm^2 for the design I that are independent of p, while a strong dependence on p is found for the values of RA_P (see Fig. 8). Values of RA_P at OCV decrease noticeably from 0.99 Ω cm^2 (design II) and/or 1.53 Ω cm^2 (design I) to 0.38 Ω cm^2 (design II) and/or 0.94 Ω cm^2 (design I), when p is increased from 0.1 MPa to 0.5 MPa. So the total impedance values of RA_{tot} (=$RA_\Omega + RA_P$) are respectively 4.66 Ω cm^2 at 0.1 MPa and/or 4.07 Ω cm^2 at 0.5 MPa under the OCV condition for the case of design I. On the other hand, at the OCV condition, the design II case using small guide vanes having a very high degree of flow uniformity in interconnectors has the values of RA_{tot} = 3.54 Ω cm^2 at 0.1 MPa and/or 2.93 Ω cm^2 at 0.5 MPa, which are about 24% (0.1 MPa) and/or 28% (0.5 MPa) smaller than that of

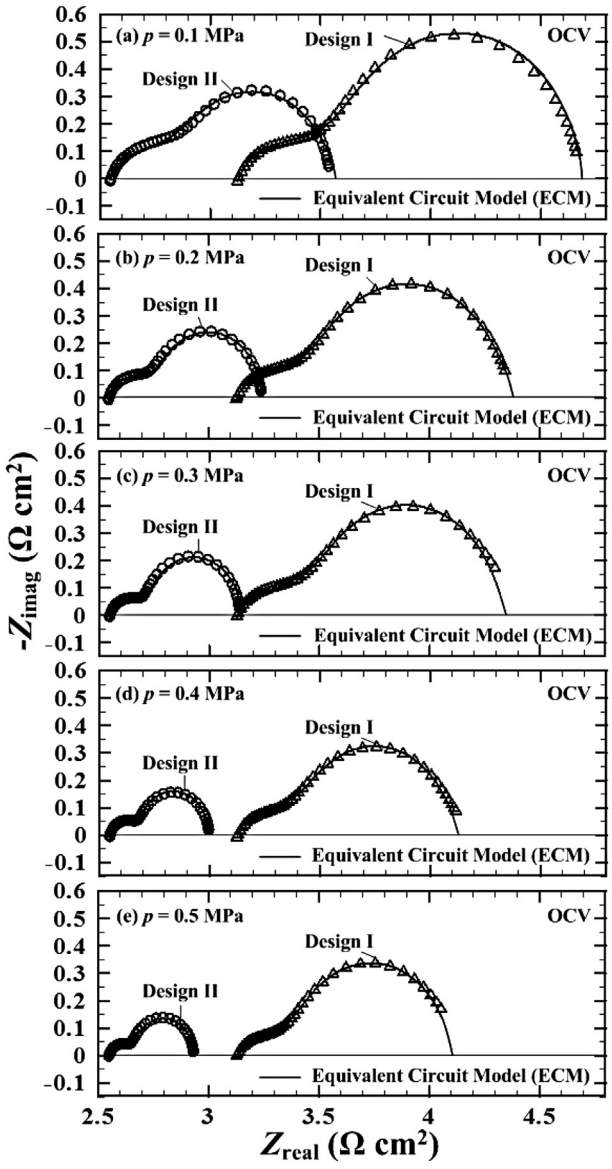

Fig. 6. Comparisons of impedance spectra (the Nyquist plots) and their ECM fitting curves measured at OCV between designs I and II under five different pressure conditions, of which the same experimental conditions are applied for both designs except using different flow distributors.

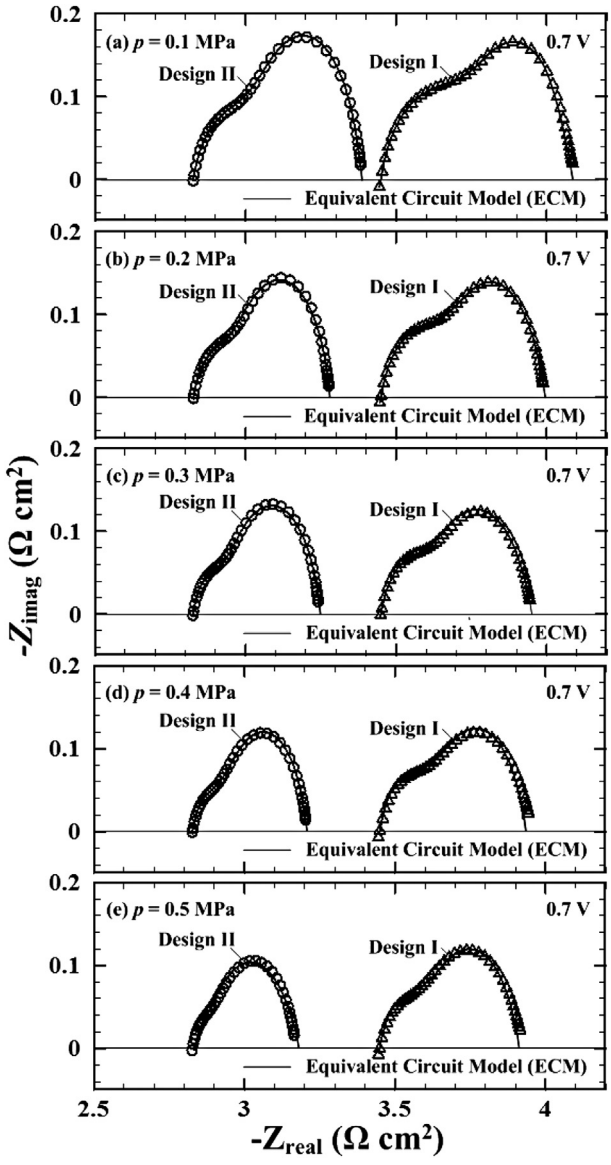

Fig. 7. Same arrangements as Fig. 6, but measured at the loaded condition when the single-cell stacks are operated at 0.7 V.

the design I case. The smaller values of RA_{Ω} and RA_{P} found in the case using the design II explain why the case of the design II has a higher value of OCV than that of the design I at any given p (see Fig. 2). The higher the OCV value found in the design II is attributed to the better flow uniformity in interconnectors because of using guide vanes.

For the loaded condition at 0.7 V, similar results are found. Fig. 9 shows that the ohmic resistance is independent of pressure, while the polarization resistance decreases noticeably with increasing pressure. Specifically, RA_{Ω} = 2.83 Ω cm^2 for the design II and RA_{Ω} = 3.45 Ω cm^2 for the design I that are unchanged with increasing pressure. But values of RA_{P} decrease from 0.56 Ω cm^2 to 0.34 Ω cm^2 for the design II and from 0.64 Ω cm^2 to 0.47 Ω cm^2 for the design I, as p increases from 0.1 MPa to 0.5 MPa at 0.7 V. Both impedance measurements at OCV and 0.7 V conditions show that pressurization has little influence on the ohmic resistance, but it has a noticeable influence on the polarization resistance where values of RA_{P} decrease with increasing p. When compared values of RA_{Ω} between the two cases at OCV (Fig. 8) and at 0.7 V (Fig. 9) for each of designs I and II (see also values of R_{Ω} in Table 1), we found that the RA_{Ω} values at 0.7 V are about 10% higher than that under the OCV condition. This is due to the increase of ohmic overpotential under loaded condition.

As to the total resistances, the cases of design I have values of RA_{tot} = 4.09 Ω cm^2 at 0.1 MPa and/or 3.92 Ω cm^2 at 0.5 MPa, which are about 17% (0.1 MPa) and/or 19% (0.5 MPa) higher than that of the design II. This impedance result explains why the better flow uniformity in flow distributors is, the better the cell performance is. Also, such performance enhancement due to the improvement of flow uniformity in interconnectors is found to be even more profound under elevated pressure conditions (see Fig. 4). These results are consistent with our previous impedance measurements under atmospheric condition [17]. Thus, it is reasonable to suggest that the design I case having non-uniform flow distributions in interconnectors may suffer the local fuel starvation that results in the anodic re-oxidation making the changes of the local anodic microstructures during the operation of PSOFC which in turn can block the mass diffusion pathway of supplied gases even under

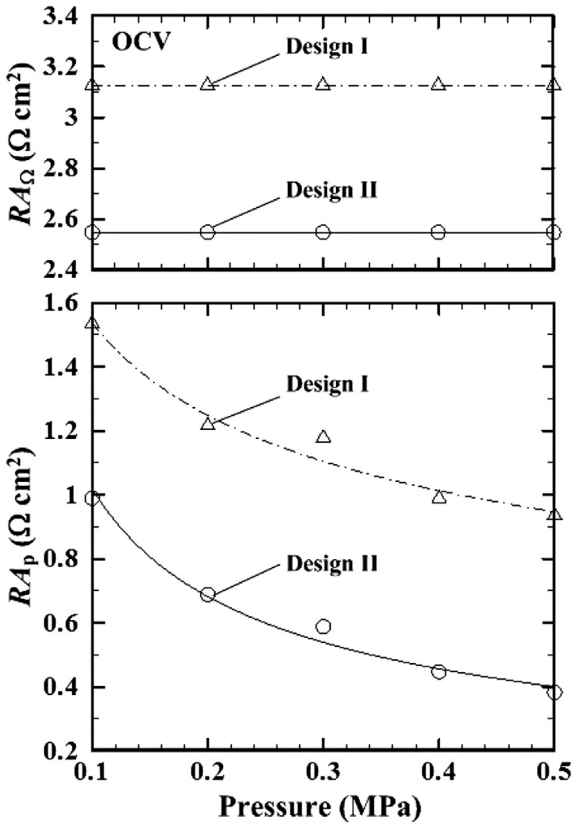

Fig. 8. Variations of ohmic and polarization resistances (RA_Ω and RA_P) with increasing pressure measured at OCV for both designs I and II cases.

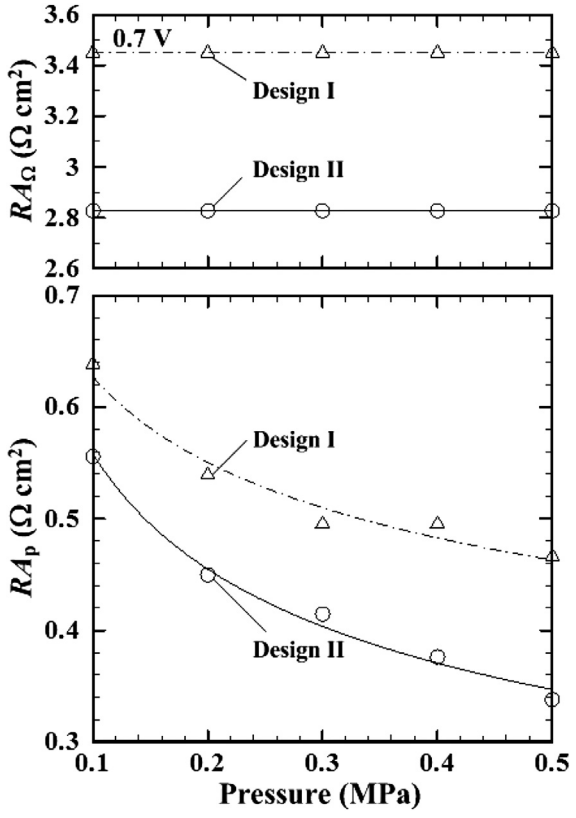

Fig. 9. Same arrangements as Fig. 8, but for the loaded condition at 0.7 V.

elevated pressure condition. On the other hand, by using simple guide vanes (design II, see Fig. 2b) to significantly improve the flow uniformity in interconnectors, the anodic surface of the PEN can remain a fully reduced metallic Ni/YSZ surface with uniform gray color (no anodic re-oxidation), please refer to Ref. [17] (Fig. 12 in Ref. [17]) for comparisons of SEM images showing different anodic microstructures of the PEN using designs I and II.

When the single-cell stack is pressurized, the density of the supplied gases is linearly increased with p, whereas the velocity of the supplied gases in interconnectors is proportionally decreased with increasing density because the mass flow rates are constant. Such a velocity decrease of the supplied gases due to pressurization can further enhance the influence of flow uniformity in interconnectors. In other words, the aforementioned local fuel starvation is more easier to occur in the design I case, because a non-uniform fuel distribution can result in a non-uniform fuel utilization on the anode and a significant drop of the fuel partial pressure, close to zero, may occur locally for some very small fuel flow velocities. As the locally anodic re-oxidation occurs where Ni is re-oxidized either by O_2 in air or by the oxide ion current, the anodic porosity can be significantly decreased by the reduction of Ni to NiO due to the volume increase of NiO which is 69% more in volume than Ni [20]. Consequently, for the design I case, the diffusion processes of hydrogen fuel in anode is to be more depressed than that of the design II case. This can lead to a smaller value of the available three-phase boundary length for the design I case. Hence, larger values of RA_Ω and RA_P are measured for the cases of design I having lower power densities than that of the design II at any p studied.

4. Conclusions

In the present study we have first introduced a novel high-pressure dual-chamber testing platform that permits direct measurements of single-cell stacks using different flow distributors. Consequently, cell performance and impedance measurements in the dual-chamber facility amenable for qualitative understanding and quantitative analysis of various aspects of electrochemical characteristics for PSOFC are obtained. In and by itself, we believe that the experimental design is a useful contribution to the PSOFC study. The present measurements and analyses reveal the following two points.

(1) Pressurization can increase the power densities of PSOFC, primarily via the decrease of the polarization resistance with increasing p because the ohmic resistance is found to be independent of p.
(2) The better flow uniformity in flow distributors is, the better the cell performance is, and such performance enhancement is found to be even more profound as p increases. This result is explained by impedance spectra data, of which both ohmic and polarization resistances for the design II case are found to be smaller than the design I case at any pressures studied upon here.

The present work provides the necessary knowledge of the electrochemical characteristics for PSOFCs. These results should be useful to the development of PSOFC integrating with micro gas turbines for future stationary power generation.

Acknowledgments

The financial supports from the National Science Council (NSC 100-2221-E-008-105-MY3) and the Institute of Nuclear Energy Research (1002001INER054) in Taiwan are greatly acknowledged.

References

[1] World Energy Outlook, International Energy Agency, Paris, France, 2011.
[2] K.R.G. Hein, Proc. Combust. Inst. 29 (2002) 393–398.
[3] S.C. Singhal, Solid State Ionics 135 (2000) 305–313.
[4] P. Costamagna, L. Magistri, A.F. Massardo, J. Power Sources 96 (2001) 352–368.
[5] W.L. Lundberg, S.E. Veyo, M.D. Moeckel, ASME J. Eng. Gas Turbines Power 125 (2003) 51–58.
[6] S.E. Veyo, L.A. Shockling, J.T. Dederer, J.E. Gillet, W.L. Lundberg, ASME J. Eng. Gas Turbines Power 125 (2003) 51–58.
[7] S.K. Park, T.S. Kim, J. Power Sources 163 (2006) 490–499.
[8] Y. Kobayashi, Y. Ando, Y. Kabata, M. Nishiura, K. Tomida, N. Matake, Mitsubishi Heavy Ind. Tech. Rev. 48 (2011) 9–15.
[9] T.H. Lim, R.H. Song, D.R. Shin, J.I. Yang, H. Jung, I.C. Vinke, S.S. Yang, Int. J. Hydrogen Energy 33 (2008) 1076–1083.
[10] L. Zhou, M. Cheng, B. Yi, Y. Dong, Y. Cong, W. Yang, Electrochim. Acta 53 (2008) 5195–5198.
[11] Y. Li, Y. Weng, J. Power Sources 196 (2011) 3824–3835.
[12] S. Seidler, M. Henke, J. Kallo, W.G. Bessler, U. Maier, K.A. Friedrich, J. Power Sources 196 (2011) 7195–7202.
[13] H. Yakabe, Y. Baba, T. Sakurai, M. Satoh, I. Hirosawa, Y. Yoda, J. Power Sources 131 (2004) 278–284.
[14] H. Yoshida, H. Yakabe, K. Ogasawara, T. Sakurai, J. Power Sources 157 (2006) 775–781.
[15] C.M. Huang, S.S. Shy, C.H. Lee, J. Power Sources 183 (2008) 205–213.
[16] C.M. Huang, S.S. Shy, H.H. Li, C.H. Lee, J. Power Sources 195 (2010) 6280–6286.
[17] S.S. Shy, C.M. Huang, H.H. Li, C.H. Lee, J. Power Sources 196 (2011) 7555–7563.
[18] V.A.C. Haanappel, M.J. Smith, J. Power Sources 171 (2007) 169–178.
[19] J.B. Jorcin, M.E. Orazem, N. Pébère, B. Tribollet, Electrochim. Acta 51 (2006) 1473–1479.
[20] T. Hatae, Y. Matsuzaki, Y. Yamazaki, Solid State Ionics 179 (2008) 274–281.